HEAT TRANSFER AND FLOW CHARACTERISTICS OF OFFSET FIN AND FLAT TUBE HEAT EXCHANGERS UNDER LOW PRESSURE ENVIRONMENT

Rui WAN[1], Yichun WANG[1,*], Revaz KAVTARADZE[1], Xinglei HE[1]

[1] School of Mechanical Engineering, Beijing Institute of Technology, Beijing, China

[*]Corresponding author, e-mail: wd12121390@outlook.com

Due to the performance degradation of the vehicle cooling system heat exchanger in the low pressure environment, the problem of overheating of the cooling system occurs when the vehicle is running on the plateau. This seriously affects the use of vehicles in the plateau environment. Therefore, it is necessary to study the influence of the plateau low pressure environment on the heat transfer and flow characteristics of the vehicle cooling system heat exchanger. In this paper, an experimental study of an offset fin and flat tube heat exchanger was conducted on a low pressure wind tunnel test bench, and the heat transfer and flow characteristics of the heat exchanger under different gauge pressure conditions were analyzed. Based on this, numerical simulations were carried out to study the heat transfer and flow characteristics of the heat exchanger with different structural parameters under low pressure environment. The empirical correlation of Colburn j factor and Friction factor f were fitted using multiple linear regression. The research results can provide help for the engineering calculation of the offset fin and flat tube heat exchanger.

Key words: offset fin; heat transfer; low pressure environment; experiment and numerical simulation

1. Introduction

With the continuous increase in the level of economic development, the demand for automotive applications in the plateau has gradually increased. For cars designed for the plain area, there are a couple of serious problems in the low-pressure environment of the plateau, including declining power performance, overheating of the engine, and overheating of the cooling system. One of the most important reasons for these problems is the performance degradation of the heat exchanger of vehicle cooling system in the plateau environment. Therefore, it is necessary to study the influence of plateau low pressure environment on heat transfer and flow characteristics of heat exchangers.

Research on the influence of low-pressure environment on the performance of heat exchangers has been published in some literatures. Tanaka[1] conducted an experimental study on the heat transfer characteristics of radiation, convection, and heat conduction processes in low pressure and low temperature environments. The results show that the Knudsen Number is an indicator of the change in the dominant heat transfer mode in the low pressure environment. Liu[2] deduced the performance of the natural convection heat exchanger under low pressure environment. The results show that the natural convective heat transfer coefficient of the flat wall at an altitude of 5000 m is reduced by 27% compared with that at the plain. Liang[3] studied the performance change of tube-fin

heat exchangers of air conditioner under different environmental pressures. Theoretical derivation shows that when the wind speed is constant, the air side convection heat transfer coefficient and the pressure drop of the heat exchanger decrease with the decrease of the ambient pressure, and the theoretical derivation conclusions are verified by experimental results. Li[4] used theoretical deduction to analyze the effect of environmental pressure on the performance of the heat exchanger. The calculation results show that the air side convection heat transfer coefficient at an altitude of 5000m decreases by 22%~33% compared with that at the plain. Jia[5, 6] studied the heat transfer and flow resistance performance of a louvered fin heat exchanger under low pressure environment. The results show that the air side convection heat transfer coefficient decreases with the decrease of the ambient pressure. Obviously, the plateau low pressure environment has a serious impact on the heat transfer performance of the air side of the heat exchanger and needs to be studied in depth.

Offset fin heat exchangers are widely used in vehicle cooling systems. At present, researchers have studied their performance under atmospheric pressure. Kays[7] first analyzed the heat transfer and flow of offset fins, and established a modified analytical solution model for the laminar flow boundary layer of offset fins. Dong[8] conducted an experimental study on 16 different offset fin heat exchanger samples, and obtained the empirical correlations of j factor and f factor in the Reynolds number range of 500-7500. Peng[9] numerically simulated the offset fins and analyzed the heat transfer and flow resistance characteristics of offset fins.

At present, research on offset fin heat exchangers has been focused on normal pressure environment, and the influence of low pressure environment on the flow and heat transfer performance of offset fin heat exchangers remains to be studied. Thus, it is of great significance to study the heat transfer and flow characteristics of the offset finned flat tube heat exchanger under the low pressure environment.

In this paper, an experimental study of an offset fin and flat tube heat exchanger (OFFTHX) was conducted on a low pressure wind tunnel test bench, and the heat transfer and flow characteristics of the OFFTHX under different gauge pressure conditions were analyzed. Based on this, numerical simulations were carried out to study the heat transfer and flow characteristics of the OFFTHX with different structural parameters under low pressure environment. The empirical correlation of Colburn j factor and Friction factor f were fitted using multiple linear regression. The research results can provide help for the engineering calculation of the OFFTHX.

2. The influence of low pressure environment

2.1 Physical properties of air and water

In this study, the physical parameters of water and air have important effects, including density, kinematic viscosity, dynamic viscosity, thermal conductivity, specific heat capacity, and boiling point of water. According to the ideal gas state equation, when the temperature is constant, the air density is inversely proportional to the ambient pressure[10]. The volumetric elastic modulus of liquid water is 2000 MPa. When the pressure variation is 101 kPa, the volume change is less than 1/20000, so the water density can be considered as a constant in this study[11]. According to the fluid molecule theory, the dynamic viscosity of air and water is independent of pressure when the temperature is constant[12]. According to the definition of kinematic viscosity, it is inversely proportional to the density of the fluid and is proportional to the dynamic viscosity of the fluid. When the dynamic viscosity is constant, the kinematic viscosity increases with the decrease of density, that is, the

kinematic viscosity of air increases with the decrease of environmental pressure. The physical properties of air under different gauge pressures[10] are shown in Table 1.

Table 1. Physical properties of air

Gauge pressure [kPa]	ρ[kgm^{-3}]	ν(m^{2}s^{-1})	c_p[Jkg^{-1}K^{-1}]	λ[Wm^{-1}K^{-1}]
0	1.1885	1.54E-05	1006.4	0.0242
-10	1.0696	1.71E-05	1006.4	0.0242
-20	0.9507	1.92E-05	1006.4	0.0242
-30	0.8319	2.19E-05	1006.4	0.0242
-40	0.7130	2.56E-05	1006.4	0.0242

According to the fluid molecules theory[12], when the temperature is constant, the thermal conductivity of water and air is constant within the pressure range of 2.67×10^{-3} - 2×10^{3}MPa. In the pressure range of 0-1 atm, the specific heat capacity of water and air can be regarded as a single-valued function of temperature[13]. In this study, the ambient pressure is within this range, and the temperature change of water and air is small, so the specific heat capacity of water and air can be regarded as constants. Environmental pressure has an effect on the boiling point of water. According to the ideal gas state equation and the Clausius Clapeyron[14] equation, the boiling point of water can be expressed as: $T_b(a)=373.15-3.3\times10^{-3}a$ [m]. According to the formula, for every 1000m increase in altitude, the boiling point of water is reduced by about 3.3 °C. At an altitude of 4500 m, the boiling point of water drops to approximately 85.15 °C.

2.2 Heat transfer and flow characteristics of heat exchangers

The thermal resistance on the air side usually accounts for more than 80% of the total thermal resistance[15]. Therefore, the air side flow and heat transfer characteristics under low pressure environment are mainly analyzed in this paper. According to the literature[5] , the thickness of the thermal boundary layer of the air flow increases with the decrease of the gas density, so the thickness of the gas thermal boundary layer under low pressure environment will increase, which will increase the thermal resistance, resulting in the convection heat transfer coefficient reduce.

3. Experimental study

3.1 Test apparatus and component parameters

The test bench used in this study is a low pressure wind tunnel test rig. The main components and structure of the test bench are shown in Figure 1. The main body of the test bench is a closed air circuit. The air circuit is equipped with a fan to drive

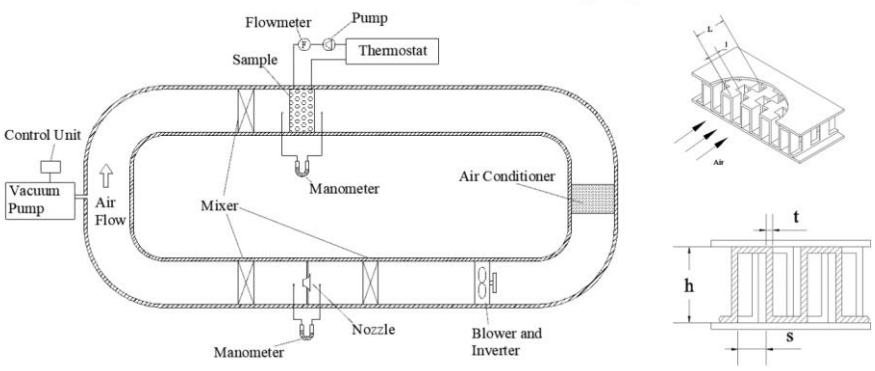

Figure 1. Schematic diagram of the wind tunnel test apparatus and offset fin structure size

the airflow. A nozzle flow meter is installed downstream of the fan, and flow stabilizers are installed before and after the flow meter. The other side of the flowmeter is a sample of the heat exchanger. The air conditioner and the flow stabilizer are installed upstream of the sample to ensure that the sample inlet air temperature and flow are uniform and stable. A vacuum pump and its control unit are connected to the air circuit for a stable low pressure environment. In order to reduce the heat loss of the air circuit, the outer wall of the circuit is wrapped with 5mm of insulation material.

In the experiment, the flow rate of water in the sample is controlled by adjusting the valve, and the water temperature at the inlet of the sample is kept constant by a constant temperature water tank. Air flow rate is controlled by adjusting the fan frequency. The pressure in the air circuit is adjusted with a pressure control system to stabilize it within ±0.1kPa of the target value.

The heat exchanger sample in the experiment is an aluminum offset fin and flat tube heat exchanger. The size of the windward surface is 185×200 mm, and its structural dimensions are shown in Figure 1. Table 2 lists the specific dimensions of the heat exchanger sample.

Table 2. Structure size of the sample

Structural parameters	L	l	h	t	s
Size[mm]	41.6	5.2	9.2	0.5	2.2

In the experiment, the inlet water temperature of the sample is maintained at 60±0.5°C, and the water flow rate is 300L/min. The inlet air temperature is maintained at 20±0.5°C. Adjust the pressure control system so that the gauge pressure in the air circuit is 0 kPa, -10 kPa, -20 kPa, -30 kPa, and -40 kPa, respectively. At each gauge pressure, the fan frequency range is 35 to 125 Hz. In order to improve the accuracy of the experimental measurements, the data is collected after each experimental condition is stabilized for 40 minutes, and the steady-state heat balance deviation is 5%.

3.2 Data reduction and error analysis

The calculation formula of the heat capacity in the experiment is:

$$Q = \left(Q_w + Q_a\right)/2 \tag{1}$$

Where Q_w and Q_a are the heat capacity of the air side and the water side, respectively.

In the heat transfer process of the finned tube, the thermal resistance is divided into three parts. Using the thermal resistance separation method, the expression of the air side convection heat transfer coefficient is[10] :

$$\frac{1}{k_a \eta_a} = \frac{1}{k} - \left(R_w + R_s + R_j + \frac{1}{k_w \cdot A_w} \right) \cdot A_a \tag{2}$$

Where, η_a is the total efficiency of rib surface, $\eta_a = \left(A_1 + \eta_f A_2\right)/A_a$. η_f is the fin efficiency, the calculation result of which is 0.783. R_w is the thermal conductivity resistance of the finned tube. R_s is fouling thermal resistance, the OFFTHX in this study is a new product, so it can be considered as R_s=0. R_j is the contact thermal resistance. Considering the processing and using environment of the finned tube in this study, the contact thermal resistance is considered to be 3×10^{-4} m^2 • K /W. k_a is the heat transfer coefficient of the air side. k_w is the heat transfer coefficient of the water side. A_w is the water side heat exchange area. The Colburn j factor of water side is calculated by the empirical correlation proposed by Guo[16].

The expressions of Colburn j factor and Fanning friction factor f are as follows:

$$j = \frac{Nu}{\mathrm{Re}\,\mathrm{Pr}^{1/3}} \tag{3}$$

$$f = \frac{de}{L} \cdot \frac{\Delta p}{\frac{1}{2}\rho u_m^2} \tag{4}$$

The relative error of the experimental data is calculated according to the estimation method. For a function R, it contains n independent variables Xi={x1,x2,…,xn}. Then the relative error expression of R is as follows:

$$\frac{\Delta R}{R} = \left[\sum_{i=1}^{n} \left(\frac{\Delta X_i}{X_i} \right)^2 \right]^{1/2} \tag{5}$$

Where, ΔX_i is the absolute error of X_i. According to the above formula, the relative errors of Colburn j factor and friction factor f are 3.48% and 5.02%, respectively.

3.3 Experimental result analysis

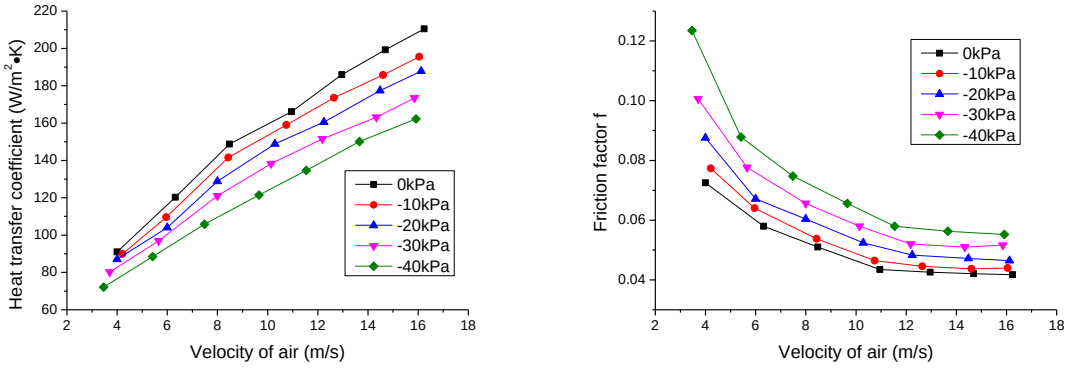

(a)Heat transfer coefficient **(b) Friction factor f**

Figure 2. Experimental results under different gauge pressure conditions

The heat transfer coefficient of offset fins under different gauge pressure conditions is shown in Figure 2(a). Under each gauge pressure condition, the convective heat transfer coefficient of the air side increases with the increase of wind speed between the fins. Under normal pressure, as the wind speed between fins increases from 3.9m/s to 16.2m/s, the air side convective heat transfer coefficient increases from 91W/m^2 • K to 210W/m^2 • K. When the wind speed between the fins is constant, the air side convective heat transfer coefficient decreases as the gauge pressure decreases. When the gauge pressure is -40 kPa, the convective heat transfer coefficient at the same wind speed is reduced by 20.9%~28.9% compared with the normal pressure. Low pressure condition has a significant effect on the convection heat transfer coefficient of the air side.

Figure 2(b) shows the friction factor f under different gauge pressure conditions. The friction factor f decreases with the increase of wind speed between the fins. Under normal pressure, as the wind speed increases from 3.9 m/s to 16.2 m/s, the friction factor f decreases from 0.072 to 0.041.

When the wind speed between the fins is constant, the friction factor f increases as the gauge pressure decreases. When the gauge pressure is -40 kPa, the friction factor f increases by 32.2%~70.3% compared with the normal pressure.

4. Numerical simulation

According to the previous analysis, the low pressure environment has an important influence on the heat transfer and flow effects of the OFFTHX. In order to further analyze the influence of the low pressure environment on the OFFTHX, numerical simulation is needed.

4.1 Dimensions of the fins

In order to further study the heat transfer and flow characteristics of offset fins under low pressure environment, 16 sets of offset fins with different size parameters are designed using orthogonal design method. The dimensional parameter variables of the fins are expressed in a dimensionless form,$\alpha = s/h, \beta = t/l, \gamma = L/l, \delta = t/s$. The dimensions of each fin is shown in Table 3.

Table 3. Parameters of the offset fins

No.	de[mm]	α	β	γ	δ	No.	de[mm]	α	β	γ	δ
1	8.33	0.2	0.05	5	0.1	9	2.50	0.33	0.05	9	0.3
2	4.90	0.2	0.1	7	0.17	10	3.26	0.33	0.1	11	0.23
3	3.62	0.2	0.15	9	0.23	11	4.42	0.33	0.15	5	0.17
4	2.77	0.2	0.2	11	0.3	12	7.51	0.33	0.2	7	0.1
5	3.42	0.27	0.05	7	0.23	13	4.20	0.4	0.05	11	0.17
6	2.62	0.27	0.1	5	0.3	14	7.14	0.4	0.1	9	0.1
7	7.87	0.27	0.15	11	0.1	15	2.38	0.4	0.15	7	0.3
8	4.63	0.27	0.2	9	0.17	16	3.10	0.4	0.2	5	0.23

The computational domain in simulation is shown in Figure 3. The air flows from the left to the channel between the fins along the X axis, and it is heated then flows out. The computational region is extended in order to ensure the accuracy of calculation. The inlet section is extended by 1.5 times of the fin length l, allowing the air to obtain a uniform velocity distribution at the entrance of the fin. The outlet section is extended by 5 times the fin length l[17].

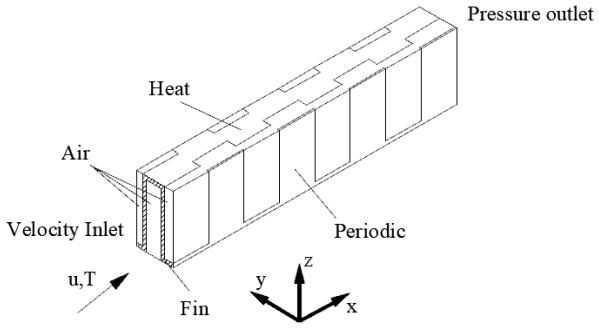

Figure 3. The computational domain

4.2 Numerical model

The main assumptions in numerical simulations are:

1) The flow in the calculation area is steady-state and incompressible;

2) Ignoring heat radiation and natural convection;

3) Physical properties of air are only related to environmental pressure.

The Reynolds number in the numerical simulation ranges from 1000 to 4000, so the laminar model is used when the Reynolds number is low, and the turbulence model is used when the Reynolds number is high. According to the reference[9], the critical Reynolds number of the air flow in the offset fin is 2000, so the turbulence model is used when the Reynolds number is greater than 2000 in the simulation.

Based on the above, the continuity equation is:

$$div\left(\rho \mathbf{u}\right)=0 \tag{6}$$

The momentum conservation equation (Laminar flow: Re<2000) is:

$$\frac{\partial}{\partial x_j}\left(u_i u_j\right)=\frac{\mu_l}{\rho_l}\nabla^2\left(u_i\right)-\frac{1}{\rho_l}\frac{\partial p}{\partial x_i} \tag{7}$$

The momentum conservation equation (turbulent flow: Re $\geqslant$ 2000) is:

$$\rho_l\frac{\partial k}{\partial t}+\rho_l u_j\frac{\partial k}{\partial x_j}=\frac{\partial}{\partial x_j}\left[\left(\mu+\frac{\mu_t}{\sigma_k}\right)\frac{\partial k}{\partial x_j}\right]+\mu_t\frac{\partial u_i}{\partial x_j}\left(\frac{\partial u_i}{\partial x_j}+\frac{\partial u_j}{\partial x_i}\right)-\rho_l\varepsilon \tag{8}$$

$$\rho_l\frac{\partial \varepsilon}{\partial t}+\rho_l u_k\frac{\partial \varepsilon}{\partial x_k}=\frac{\partial}{\partial x_k}\left[\left(\mu+\frac{\mu_t}{\sigma_\varepsilon}\right)\frac{\partial \varepsilon}{\partial x_k}\right]+\frac{c_1\varepsilon}{k}\mu_t\frac{\partial u_i}{\partial x_j}\left(\frac{\partial u_i}{\partial x_j}+\frac{\partial u_j}{\partial x_i}\right)-c_2\rho_l\frac{\varepsilon^2}{k} \tag{9}$$

The energy conservation equation is:

$$div\left(\rho T\mathbf{u}\right)=div\left(\frac{\mu}{\mathrm{Pr}}gradT\right)+S_T \tag{10}$$

4.3 Mesh and boundary conditions

The computational domain is divided into tetrahedral meshes, and the mesh at the wall surface is encrypted to improve the accuracy of numerical calculations.

Different numbers of meshes are calculated for the computational domain, and the number of meshes is increased from 0.1 to 2.02 million. When the number of grids is increased from 650,000 to 1.15 million, the change of temperature and pressure difference between the inlet and outlet are less than 0.3%. Therefore, after the number of grids exceeds 650,000, the calculation result is independent to the number of grids. The tetrahedral mesh size is 0.25mm.

The upper and lower surfaces of the computational domain are heating surfaces, and the temperature is 323.15K. The left and right boundaries of the computational domain are set to periodic boundaries. The air inlet is set to the velocity inlet, the air inlet temperature is 288.15K, and the inlet velocity is calculated based on the Reynolds number. The air outlet is set as a pressure outlet.

The governing equations are solved numerically by using a control volume based finite difference formulation. The simple algorithm is used to solve iteratively the system of finite-difference equations. The second-order upwind scheme is adopted to solve the governing equations.

The offset fins are made of aluminum, the density of which is 2700 kg/m^3, and the thermal conductivity of which is 237.2W/ (m·K). The physical properties of air changes with the environmental pressure, and are shown in Table 1.

In the numerical simulation, the gauge pressure is taken as 0 kPa, -10 kPa, -20 kPa, -30 kPa, and -40 kPa. The air inlet Reynolds number ranges from 1000 to 4000 under each pressure condition.

4.4 Validation of numerical calculation model

In order to verify the accuracy of the numerical calculation model, the offset fin in the experiment is simulated. The numerical results are compared with the experimental data, as shown in Figure 4.

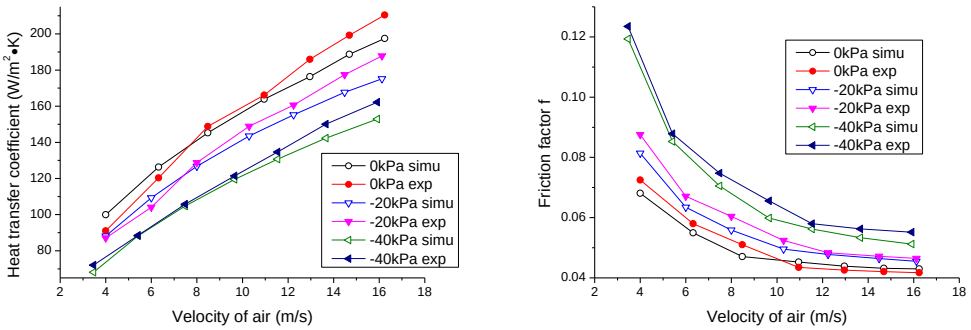

(a) Heat transfer coefficient **(b) Friction factor f**

Figure 4. Comparison of numerical results and experimental data

Figure 4(a) shows the air side convection heat transfer coefficient k_a and Figure 4(b) shows the friction factor f. The numerical simulation results are consistent with the trend of the experimental data. The maximum deviations of k_a and f between the calculation results and the experimental data are 9.7% and 7.7%, respectively, and the average deviations are 4.1% and 4.7, respectively.

4.5 Numerical simulation result analysis

4.5.1 Field synergy angle

The conventional theory holds the opinion that heat transfer enhancement should be achieved by perturbing the thermal boundary layer and the flow boundary layer, such as add vortex generators in the flow field. However, field synergy theory considers that the enhancement of heat transfer should focus on the reduction of field synergy angle[18].

The expression of the inner product of velocity and temperature gradient is:

$$\vec{U} \cdot grad\vec{T} = \left|\vec{U}\right| \cdot grad\left|\vec{T}\right| \cdot \cos\theta \tag{11}$$

Where θ is the angle between the local velocity and the temperature gradient. θ is called the field synergy angle (FSA). The diagram of the field synergy angle is shown in the Figure 5.

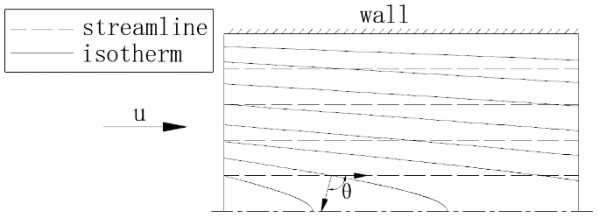

Figure 5. Diagram of the field synergy angle (FSA)

The expressions of local field synergy angle and mean field synergy angle are as follows[19]:

$$\theta_i = \cos^{-1}\left|u\frac{\partial T}{\partial x} + v\frac{\partial T}{\partial y} + w\frac{\partial T}{\partial z}\right| \Big/ \left|\vec{U}\right| \cdot \left|grad\vec{T}\right| \tag{12}$$

$$\theta_m = \sum A_i \theta_i / \sum A_i \tag{13}$$

Where A_i is the area of the control volume, θ_i is the field synergy angle of a single node, and θ_m is the mean field synergy angle of the computational domain.

Figure 6 shows the variation of the average field synergy angle (FSA) of the calculated area under different gauge pressure conditions and wind speed between fins. In the calculated wind speed range, the increase in wind speed enhances the synergy between the temperature field and the velocity, thereby enhancing the convective heat transfer between the air and the fin. The decrease of the environmental pressure increases the field synergy angle, weakens the synergy between the temperature field and the velocity, and reduces the convective heat transfer performance between the air and the fin. This is consistent with the trend of the convective heat transfer coefficient of the air side in the experiment.

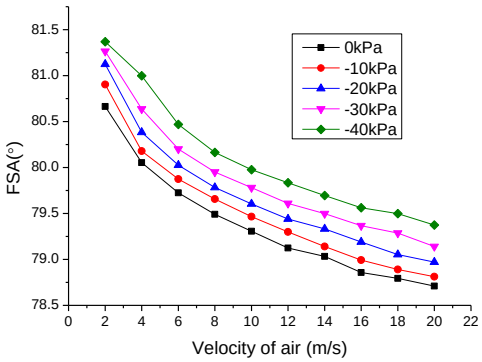

Figure 6. Average field synergy angle (FSA)

4.5.2 Correlations of j and f factors

In order to facilitate the calculation of engineering, empirical correlations of j factor and f factor are obtained by multiple linear regression[20] on the basis of the 336 operating points calculated in this paper. The corresponding correlations of the Colburn j factor and Friction factor f are given as follows:

$$j = 1.429\,\mathrm{Re}^{-0.487}\,\alpha^{-0.0557}\beta^{0.499}\gamma^{-0.357}\delta^{-0.532}\left(P/P_0\right)^{0.0637} \tag{14}$$

$$f = 20.493\,\mathrm{Re}^{-0.238}\,\alpha^{-0.0175}\beta^{0.725}\gamma^{-0.232}\delta^{-0.501}\left(P/P_0\right)^{-0.225} \tag{15}$$

Where P is the ambient pressure (kPa), P_0 is the standard atmospheric pressure (101 kPa).

Figure 7 shows the comparison between numerical simulation results of j factor and f factor and that of correlation calculation results. Eq.(14) can predict 95% of the simulation results of Colburn j factor within the deviation range of $\pm 10\%$. Eq.(15) can predict 95% of the simulation results of Friction factor j within the deviation range of $\pm 15\%$. The mean deviation and average deviation are calculated according to Eq.(16) and Eq.(17)[20] . The mean deviation of Eq.(14) and Eq.(15) are 4.7% and 7.8%, and the average deviation are 1.9% and 0.5%, respectively.

$$AverageDeviation = \frac{1}{N}\left(\sum \frac{\phi_{cor} - \phi_{sim}}{\phi_{sim}}\right) \times 100\% \tag{16}$$

$$MeanDeviation = \frac{1}{N}\left(\sum \frac{\left|\phi_{cor} - \phi_{sim}\right|}{\phi_{sim}}\right) \times 100\% \tag{17}$$

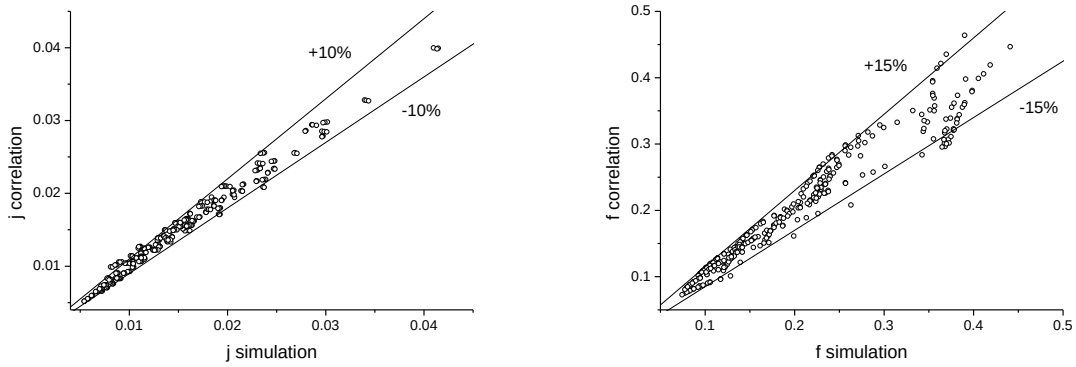

(a) j factor **(b) f factor**

Figure 7. Comparison of numerical result and correlation for j and f factor

In Figure 8, calculation results of the correlations proposed in this paper are compared with experimental data of other offset fins. Dong conducts an experimental study on offset fins of different sizes, one of the fins is code No.11. The calculation results of the correlations show good consistency with experimental data. The mean deviation of j factor is 8.2%, and that of f factor is 12.3%.

5. Conclusions

In this paper, the experimental study and numerical simulation of the heat transfer and flow resistance performance of the offset fin flat tube heat exchanger under low pressure environment were carried out. The conclusions are as follows:

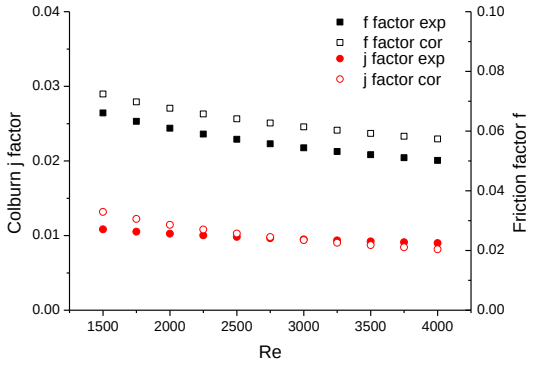

Figure 8. Comparison of present correlation and other experimental result

1. The low pressure environment has an important influence on the physical properties of air and water. When the gauge pressure is -40 kPa, the density of air is reduced by about 40% compared to when the gauge pressure is 0 kPa, and the kinematic viscosity of air is increased by about 66%.

2. The experimental results show that when the gauge pressure is -40 kPa, the convective heat transfer coefficient at the same wind speed is reduced by 20.9%~28.9% compared with the atmospheric pressure. And the friction factor f is increased by 32.2% to 70.3%.

3. The increase of wind speed enhances the synergy between temperature field and velocity, and thus enhances the convective heat transfer between air and fin. The decrease of the environmental pressure weakens the synergy between the temperature field and the velocity, and reduces the convective heat transfer performance between the air and the fin.

4. Based on the simulation results, the empirical correlations of j factor and f factor are obtained by multiple linear regression. The correlation prediction bias is reasonable, which can provide a basis for the engineering calculation of offset fins in the plateau low pressure environment.

Nomenclature

A_w	-	the water side heat exchange area, [m^2]
c_p	-	constant-pressure specific heat of air, [$Jkg^{-1}K^{-1}$]
f	-	Fanning friction factor
h	-	fin height, [mm]
j	-	Colburn j factor
k	-	heat transfer coefficient, [$Wm^{-2}K^{-1}$]
k_a	-	the heat transfer coefficient of the air side, [$Wm^{-2}K^{-1}$]
k_w	-	the heat transfer coefficient of the water side, [$Wm^{-2}K^{-1}$]
L	-	length of the fin, [mm]
l	-	flow length, [mm]
Nu	-	Nusselt number
P	-	the ambient pressure, [kPa]
P_0	-	the standard atmospheric pressure, [kPa]
Q_a	-	the heat capacity of the air side, [W]
Q_w	-	the heat capacity of the water side, [W]
Re	-	Reynolds number
R_j	-	the contact thermal resistance, [m^2KW^{-1}]
R_s	-	fouling thermal resistance, [m^2KW^{-1}]
R_w	-	the thermal conductivity resistance of the finned tube, [m^2KW^{-1}]
s	-	fin pitch, [mm]
t	-	fin thick, [mm]
	-α	s/h
	-β	t/l
	-γ	L/l
	-δ	t/s
	-η_a	the total efficiency of rib surface
	-η_f	the fin efficiency
	-θ	the field synergy angle, [°]
	-θ_i	the field synergy angle of a single node, [°]
	-θ_m	the mean field synergy angle of the computational domain, [°]
	-λ	heat transfer coefficient, [$Wm^{-1}K^{-1}$]
	-ρ	density of air, [kgm^{-3}]
	-ν	kinematic viscosity of air, [m^2s^{-1}]

References

[1] Tanaka, Y., *et al.*, Heat transfer characteristics under cryogenic, low pressure environments, *Physica C-Superconductivity and Its Applications*, *469*. (2009), 15-20, pp. 1862-1865, DOI No. 10.1016/j.physc.2009.05.127

[2] Liu, Y.D., *et al.*, Study of the heat transfer performance of a plate electric heater at low barometric pressure, *Fluid Mach*, *32*. (2004), 6, pp. 56-59

[3] Liang, B., Study on the Influence of Low Pressure Environment on the Performance of Tube-Fin Heat Exchanger for Air Conditioner, Qingdao Institute of Technology, Qingdao,2007.

[4] Li, Y., *et al.*, Calculating heat transfer of radiators for plateau vehicles, *J. Huazhong Univ. Sci. Technol. (Nat. Sci. Ed.)*, *9*. (2009), pp. 90-93

[5] Jia, R.Z., *et al.*, Research on the heat transfer and flow characteristics of fin-tube exchanger under low pressure environment, *Applied Thermal Engineering*, *112*. (2017), pp. 1163-1171, DOI No. 10.1016/j.applthermaleng.2016.06.137

[6] Jia, R.Z., *et al.*, Research on the heat and mass transfer characteristics of fin-tube exchanger under low pressure environment, *Applied Thermal Engineering*, *115*. (2017), pp. 692-701, DOI No. 10.1016/j.applthermaleng.2017.01.012

[7] Kays, W.M.,A.L. London, *Compact Heat Exchangers. 3rd Edition*. McGraw-Hill. New York, 1998.

[8] Dong, J., *et al.*, Air-side thermal hydraulic performance of offset strip fin aluminum heat exchangers, *Applied Thermal Engineering*, *27*. (2007), 2, pp. 306-313, DOI No. https://doi.org/10.1016/j.applthermaleng.2006.08.005

[9] Peng, H., *et al.*, Performance investigation of an innovative offset strip fin arrays in compact heat exchangers, *Energy Conversion and Management*, *80*. (2014), pp. 287-297, DOI No. 10.1016/j.enconman.2014.01.050

[10] Yang, S.M.,W.Q. Tao, *Heat Transfer(Fourth Edition)*. Higher Education Press. Beijing, 2006.

[11] Wu, W.Y., *Fluid mechanics*. Peking University Press. Beijing, 1982.

[12] J.H.Wan, *Theory and Properties of Fluid Molecules*. Harbin Engineering University Press. Harbin, 1994.

[13] Chen, Z.Q., *Lecture on Heat Transfer*. Higher Education Press. Beijing, 1989.

[14] Chen, W., Research and application of small high temperature heat pipe, *Energy Res. Util.*, *6*. (2000), pp. 28-31

[15] Liang, Y.Y., *et al.*, Experimental and simulation study on the air side thermal hydraulic performance of automotive heat exchangers, *Applied Thermal Engineering*, *87*. (2015), pp. 305-315, DOI No. 10.1016/j.applthermaleng.2015.05.018

[16] Guo, L.H., *et al.*, Empirical correlations for lubricant side heat transfer and friction characteristics of the HPD type steel offset strip fins, *International Communications in Heat and Mass Transfer*, *35*. (2008), 3, pp. 251-262, DOI No. 10.1016/j.icheatmasstransfer.2007.07.006

[17] Qu, Z.G., *et al.*, Three-dimensional numerical simulation on laminar heat transfer and fluid flow characteristics of strip fin surface with x-arrangement of strips, *Journal of Heat Transfer-Transactions of the Asme*, *126*. (2004), 5, pp. 697-707, DOI No. 10.1115/1.1798971

[18] Guo, Z.Y., *et al.*, The field synergy (coordination) principle and its applications in enhancing single phase convective heat transfer, *International Journal of Heat and Mass Transfer*, *48*. (2005), 9, pp. 1797-1807, DOI No. https://doi.org/10.1016/j.ijheatmasstransfer.2004.11.007

[19] Bi, C., *et al.*, Heat transfer enhancement in mini-channel heat sinks with dimples and cylindrical grooves, *Applied Thermal Engineering*, *55*. (2013), 1-2, pp. 121-132, DOI No. 10.1016/j.applthermaleng.2013.03.007

[20] Ding, Z.L., *Error Theory and Data Processing*. Harbin Institute of Technology Press. Harbin, 2002.